Supporting information

Coordinated Regulation of Phosphorous/Nitrogen Doping in Fullerene-Derived Hollow Carbon Spheres and Their Synergistic Effect for Oxygen Reduction Reaction

Fancang Meng,[a#] Suwei Wang,[b#] Bohong Jiang,[a] Li Ju,[a] Haijiao Xie,[c] Wei Jiang,[b*] Qingmin Ji[a*]

a Herbert Gleiter Institute for Nanoscience, School of Materials Science and Engineering, Nanjing University of Science & Technology, 200 Xiaolingwei, Nanjing, 210094, China

b National Special Superfine Powder Engineering Technology Research Center, Nanjing University of Science and Technology, 200 Xiaolingwei, Nanjing, 210094, China

c Hangzhou Yanqu Information Technology Co., Ltd., Building 2, Xixi Legu Creative Pioneering Park, No. 712 Wen'er West Road, Hangzhou, 310003, China

# These authors contributed this work equally

*Corresponding author: jiqingmin@njust.edu.cn, superfine_jw@126.com

Additional experimental information

Characterizations. Scanning electron microscopy (SEM) was performed on Hitachi SU8100 operating at 5 kV. Transmission electron microscopy (TEM) was performed by using FEI Talos F200X G2 operating at 200 kV. X-ray diffraction (XRD) patterns were obtained using a Bruker-AXS D8 Advance diffractometer. Raman spectra were recorded on scattering Raman spectrometer of Lanram HR Evo. Nitrogen sorption measurements were conducted on powder samples at 77K using an Autosorb-1 surface area and pore size analyzer (Gemini VII 2390). The specific surface area was calculated using Brunauer Emmett Teller method (BET). X-ray photoelectron spectroscopy (XPS) (Thermo Scientific K-Alpha) was used for the analysis of element/chemical states in the solid samples.

Simulation calculation. Structure optimization of various geometries based on density functional theory (DFT) were carried out with B3LYP functional[s1-s3] and 6-31g** basis set[s4,s5]. In order to describe the solvation effect, the SMD (Solvation Model Based on Density) implicit solvent model was used in all calculations[s6]. The vibrational frequency analysis was carried out for the optimized structure with the same calculation method to obtain the zero-point energy and free energy corrections. In order to obtain the electron energy with higher accuracy which has the major impact on the accuracy of Gibbs free energy, a single point calculation for the optimized structure with m062x functional[S7] and def2TZVP basis set[s8] was performed. The single point energy is added to the free energy correction calculated before to obtain the Gibbs free energy. All these DFT calculations were performed using Gaussian 16 program suite[s9]. The

energy of electron can not be calculated directly, therefore the indirect method of computational hydrogen electrode was applied here to calculate the Gibbs free energy change of each electrochemical reaction step[s10].

Additional data

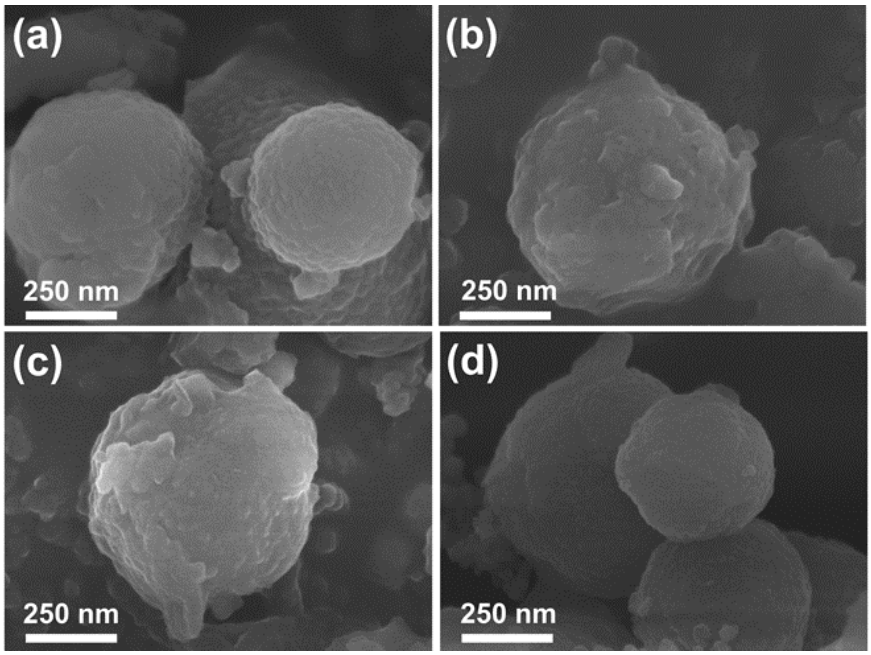

Figure S1. SEM images of (a) NP^1@FHS, (b) NP^2@FHS, (c) NP^3@FHS and (d) NP^4@FHS.

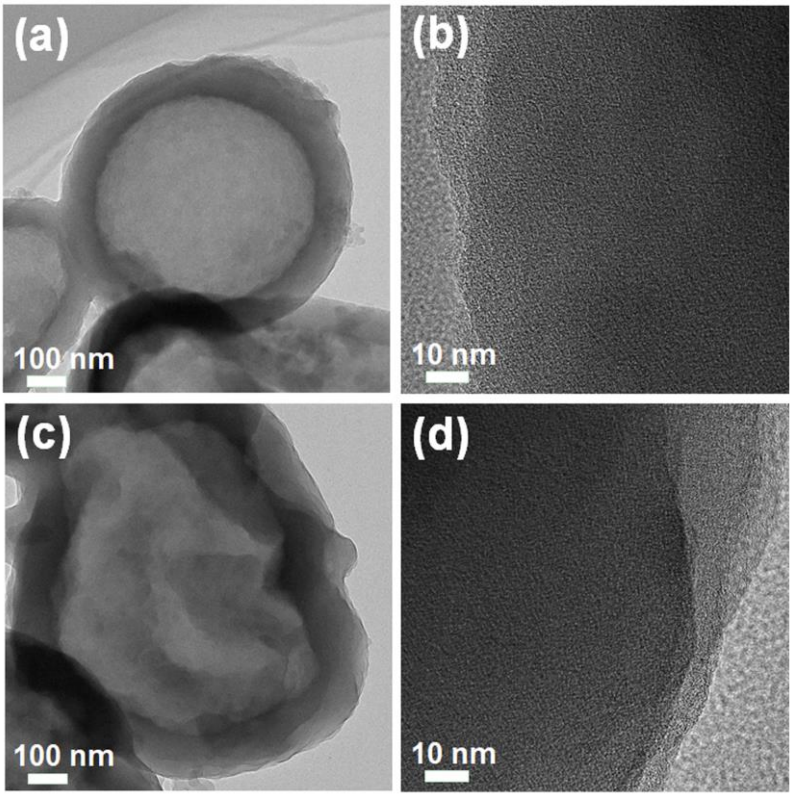

Figure S2. TEM and HR-TEM images of (a), (b) N@FHS and (c), (d) NP^3@FHS.

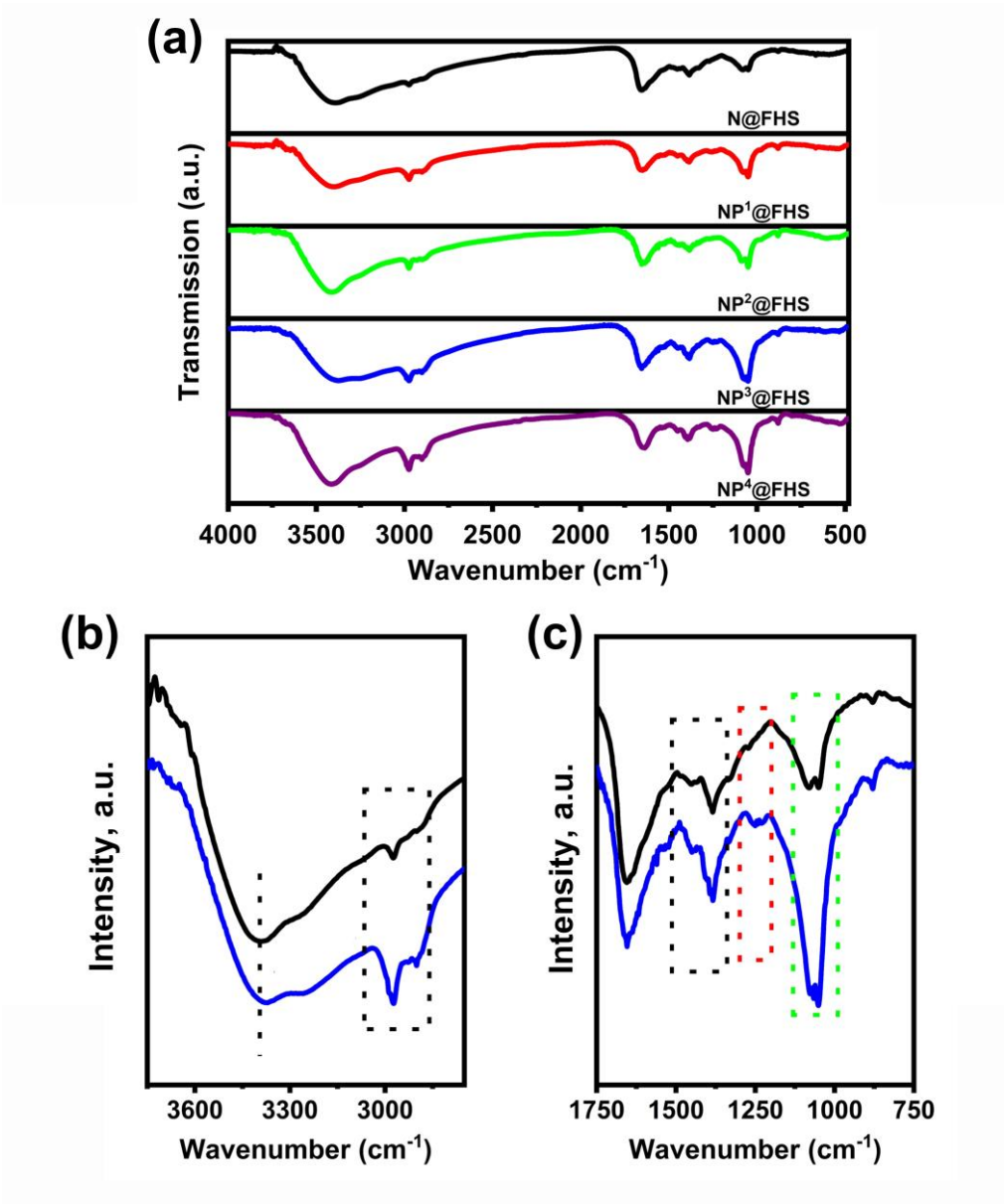

Figure S3. (a) FTIR spectra of N@FHS and NP@FHSs; (b), (c) the locally enlarged FTIR spectra of N@FHS and NP@FHS.

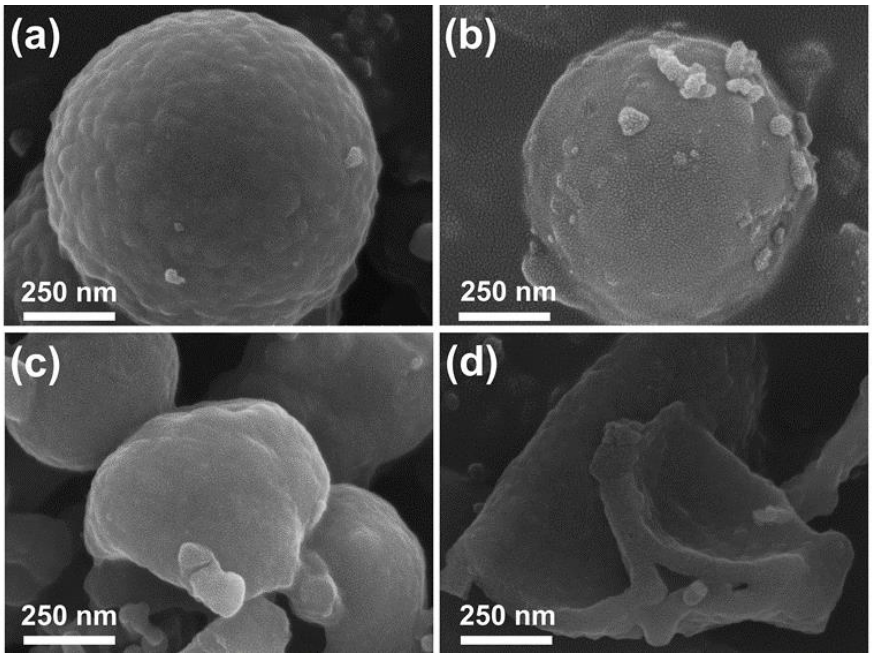

Figure S4. SEM images of (a)N@CHS, (b)NP[1]@CHS, (c) NP[2]@CHS and (d) NP[4]@CHS.

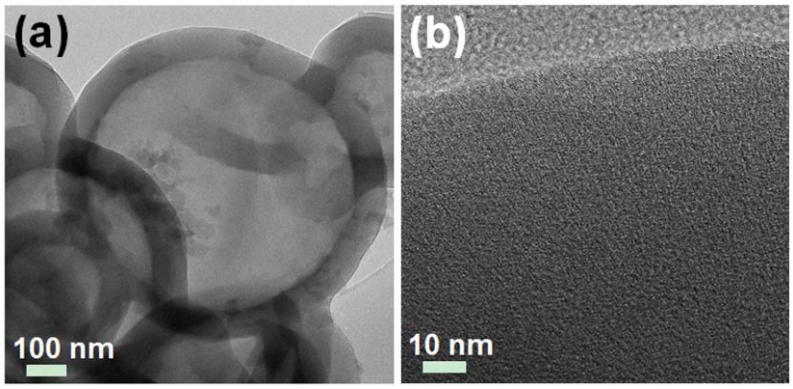

Figure S5. TEM (a) and HR-TEM (b) images of N@CHS.

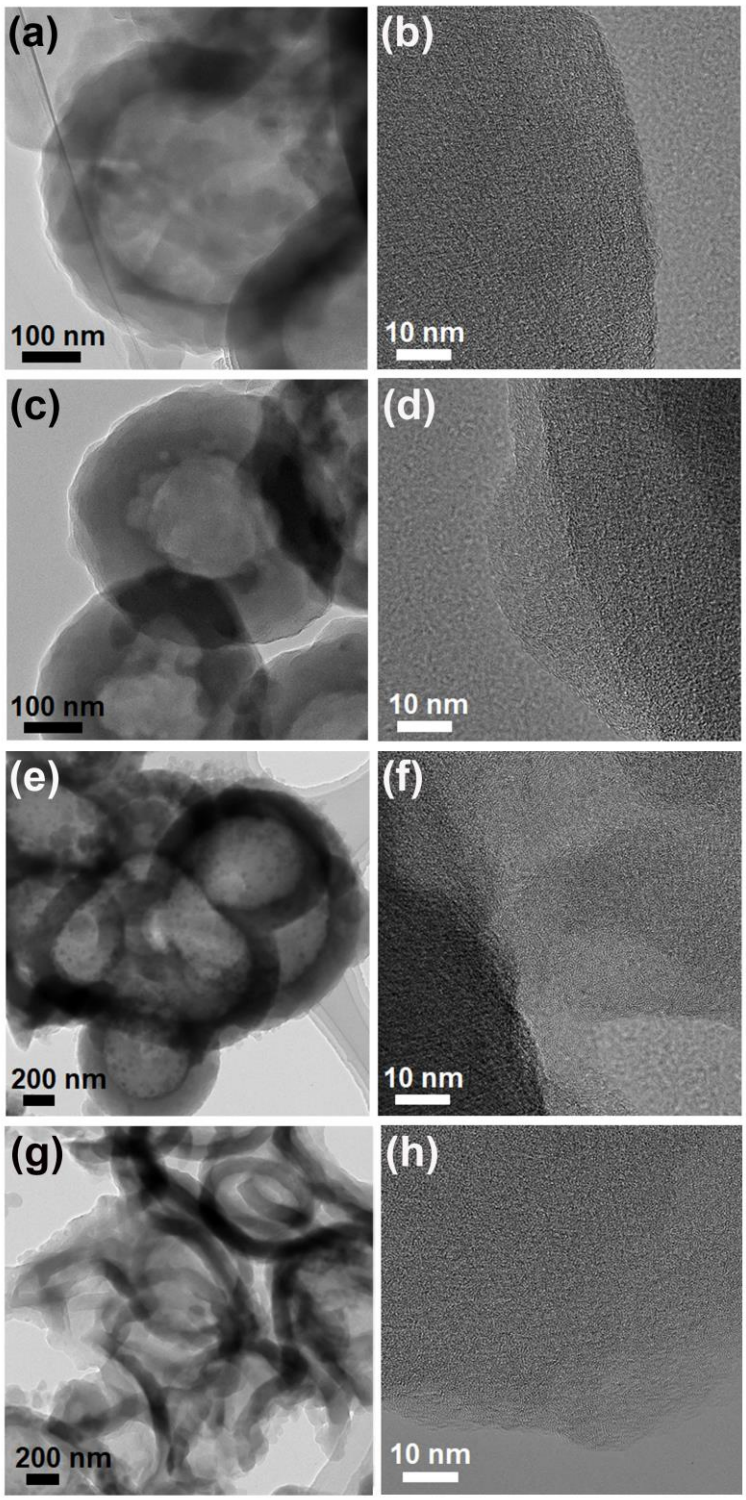

Figure S6. TEM and HR-TEM images of (a), (b) NP^1@CHS; (c), (d) NP^2@CHS; (e) (f) NP^3@CHS; and (g), (h) NP^4@CHS.

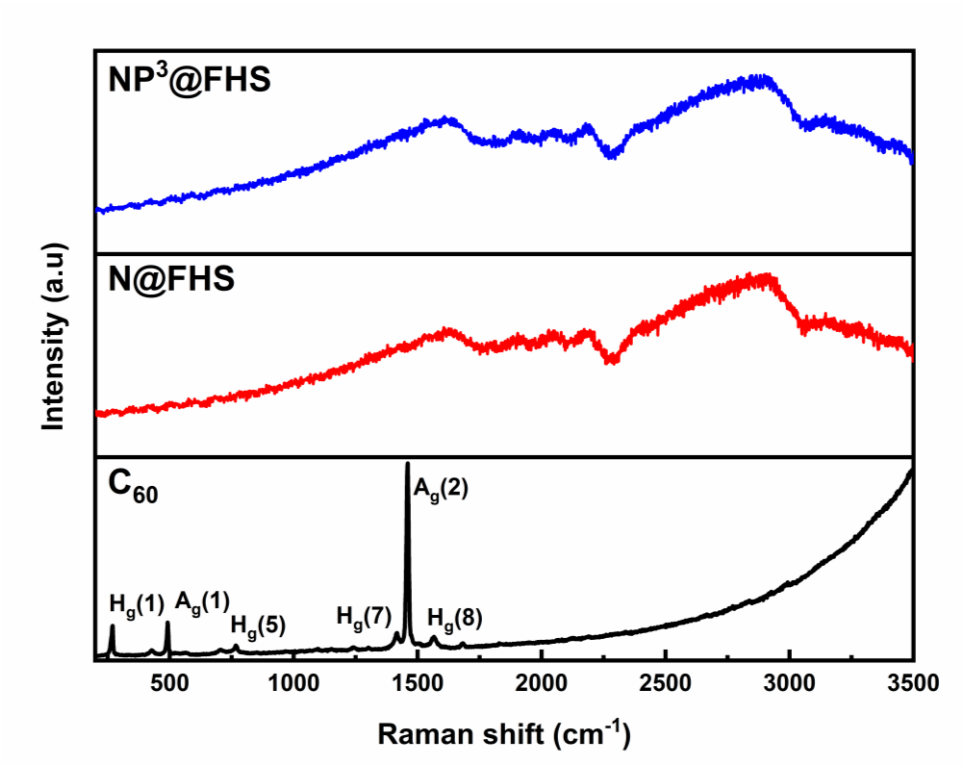

Figure S7. Raman spectra of C_{60}, N@FHS and NP^3@FHS.

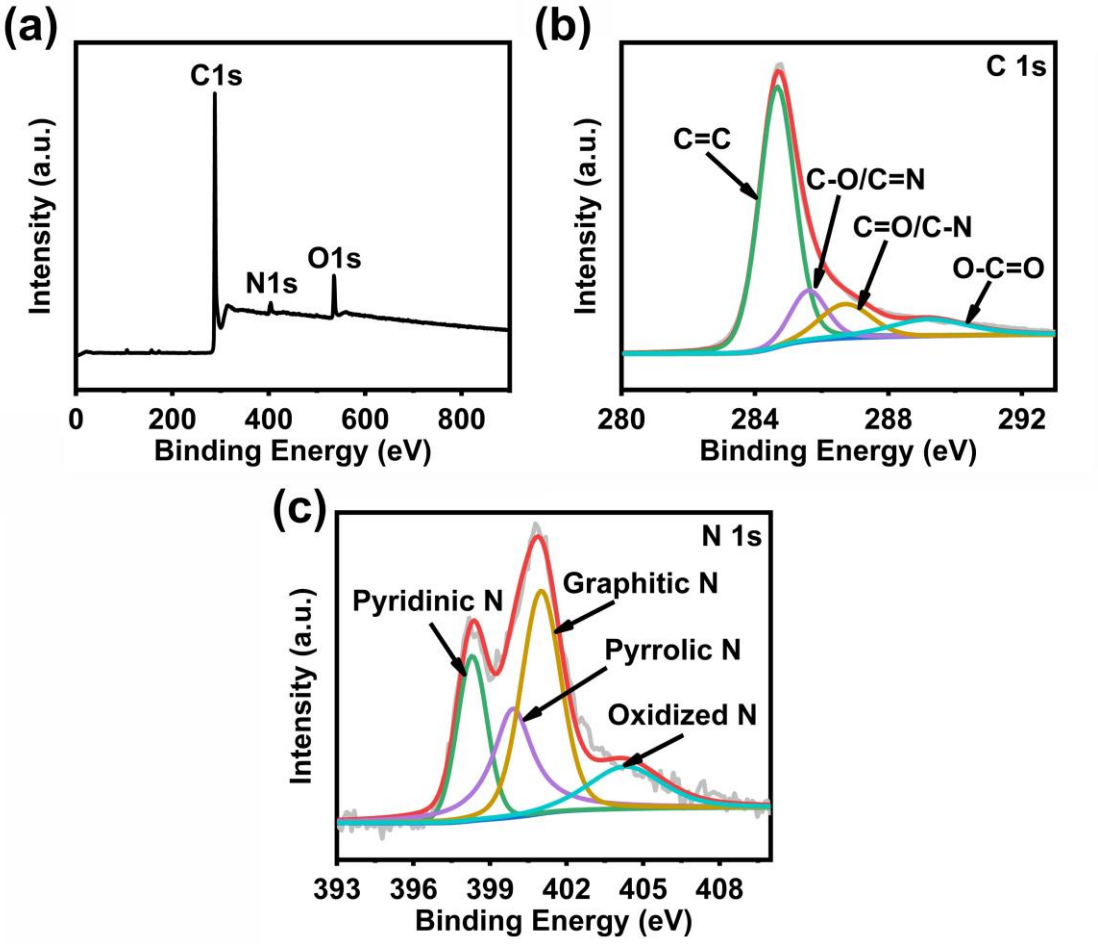

Figure S8. (a) XPS survey spectrum of N@CHS; (b) the high-resolution C 1s XPS of N@CHS; (c) the high-resolution N 1s XPS of N@CHS.

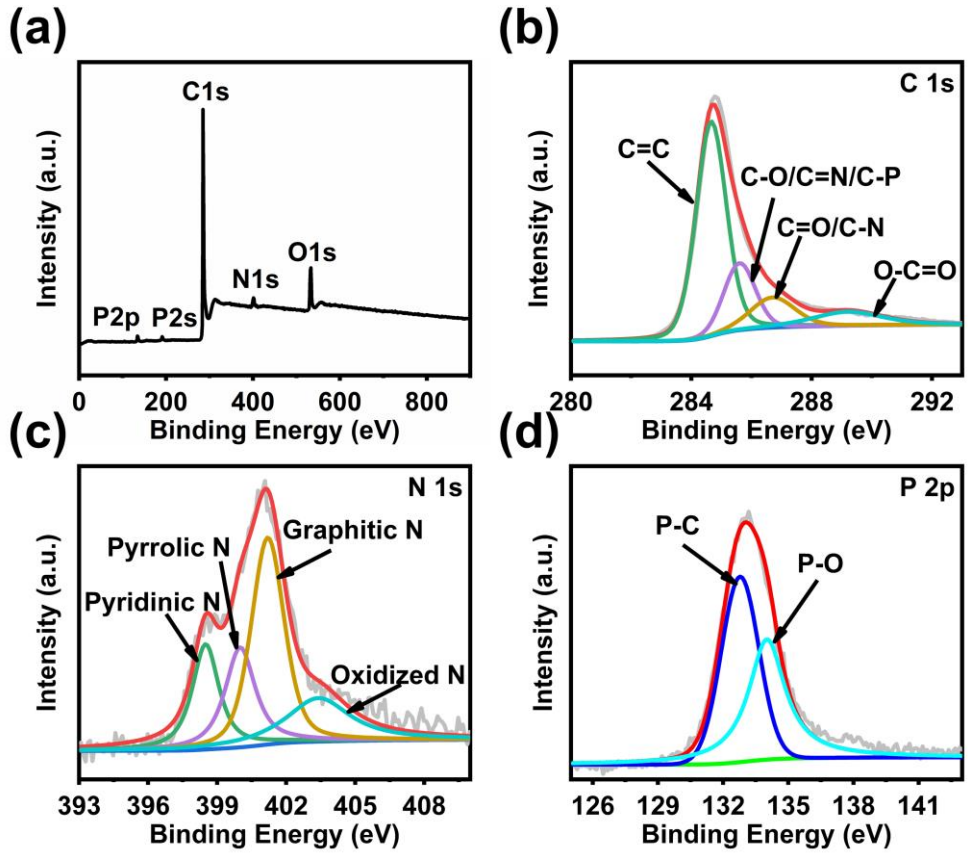

Figure S9. (a) XPS survey spectrum of NP^1@CHS; (b) the high-resolution C 1s XPS of NP^1@CHS; (c) the high-resolution N 1s XPS of NP^1@CHS; (d) the high-resolution P 2p XPS of NP^1@CHS.

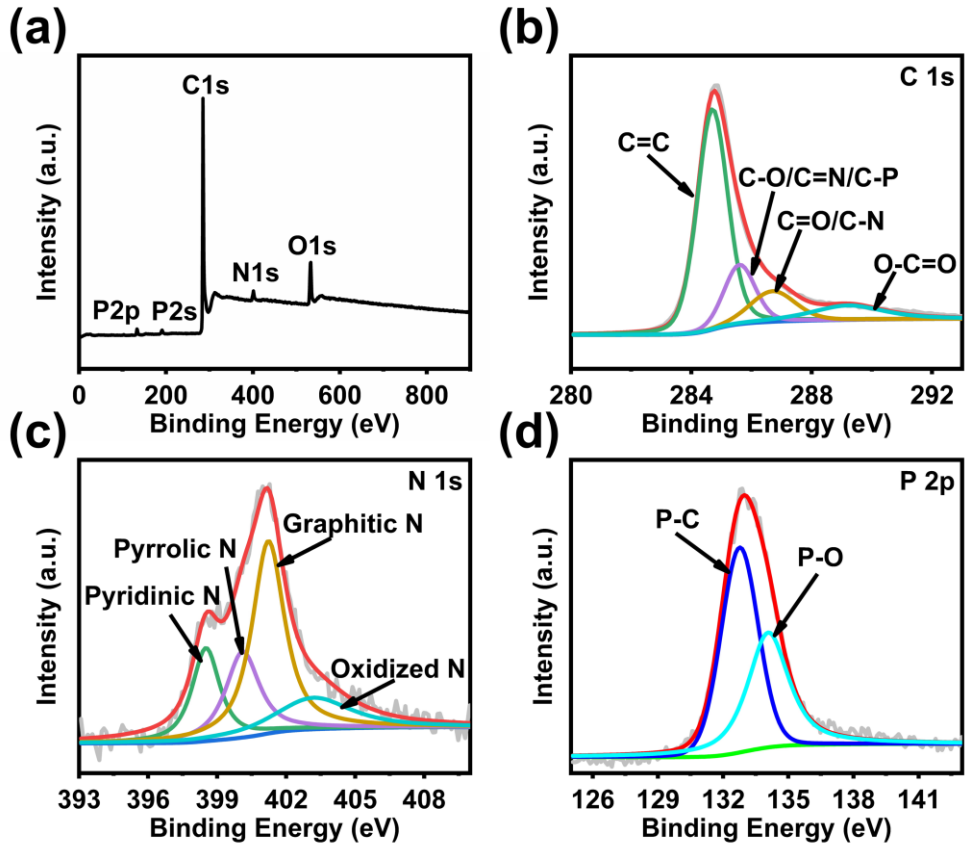

Figure S10. (a) XPS survey spectrum of NP^2@CHS; (b) the high-resolution C 1s XPS of NP^2@CHS; (c) the high-resolution N 1s XPS of NP^2@CHS; (d) the high-resolution P 2p XPS of NP^2@CHS.

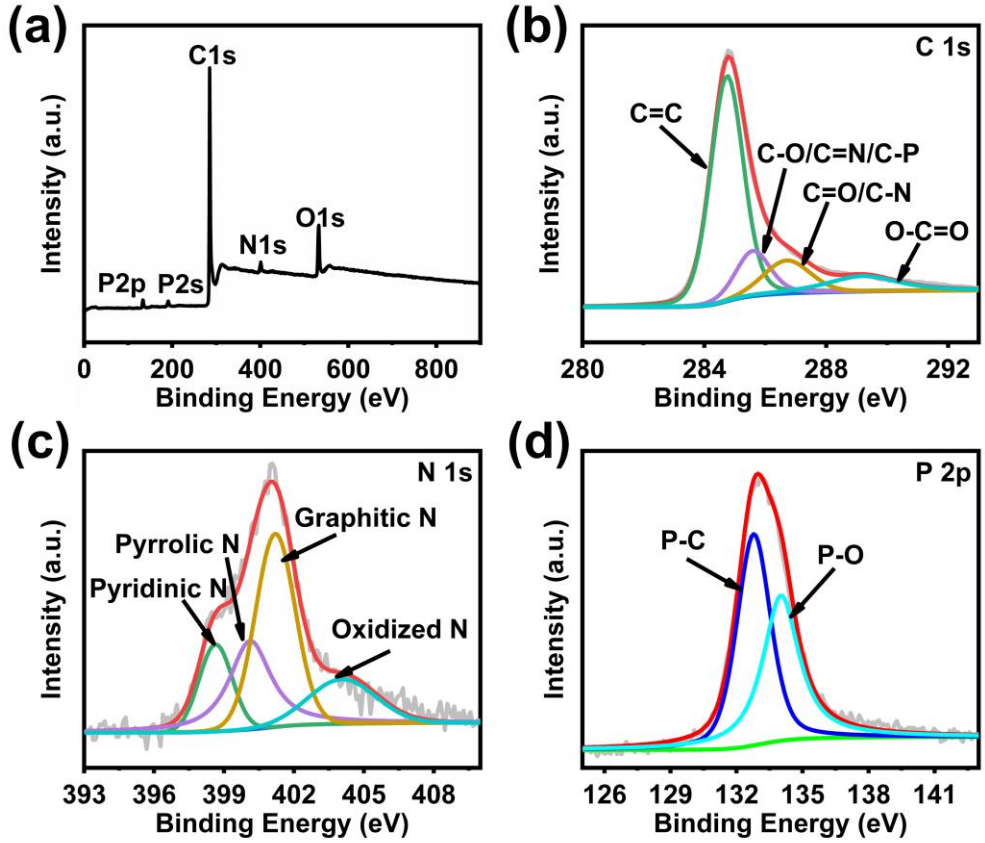

Figure S11. (a) XPS survey spectrum of NP^4@CHS; (b) the high-resolution C 1s XPS of NP^4@CHS; (c) the high-resolution N 1s XPS of NP^4@CHS; (d) the high-resolution P 2p XPS of NP^4@CHS.

.

Table S1. The content and type of N and P species in N@CHS and NP@CHSs calculated based on XPS results

Sample	N%					P%		
	Total	Oxidized N	graphitic N	pyrrolic N	pyridinic N	Total	P-C	P-O
N@CHS	8.64	14.75	38.85	25.92	20.48			
NP[1]@CHS	4.45	19.83	40.19	20.65	19.33	2.63	51.46	48.54
NP[2]@CHS	4.35	16.88	44.19	20.55	18.38	2.72	55.82	44.18
NP[3]@CHS	3.44	10.21	55.29	17.97	16.53	2.88	57.91	42.09
NP[4]@CHS	4.64	15.85	41.45	27.42	15.28	3.46	54.27	45,73

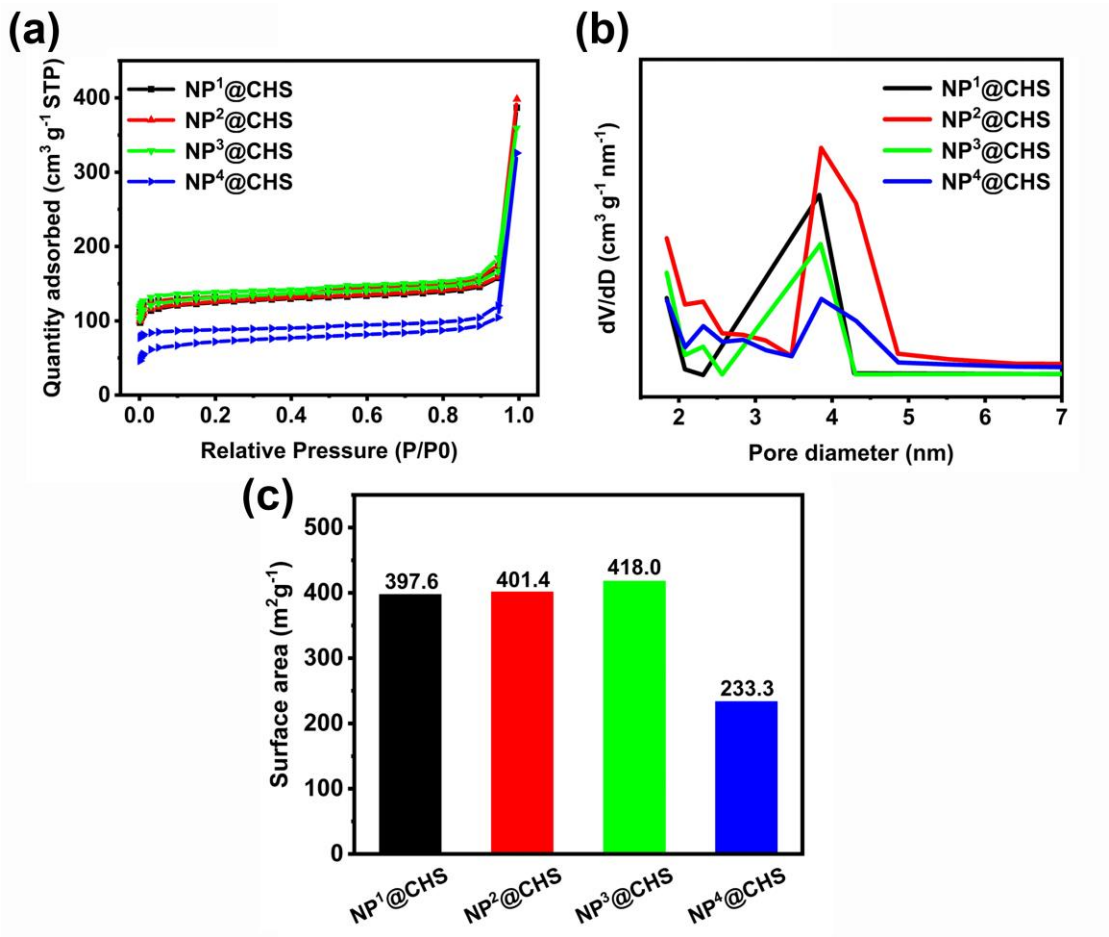

Figure S12. (a) N_2 sorption isotherms, (b) pore size distribution curves and the BET surface areas of NP@CHSs.

Table S2. Comparison of ORR activities of N@CHS, NP@CHSs and Pt/C

Sample	E_0 **(V)**	$E_{1/2}$ **(V)**	j_L**(mA·cm^{-2})**
C_{60}CS	0.763	0.632	2.611
N@CHS	0.791	0.667	3.630
NP^1@CHS	0.891	0.742	4.921
NP^2@CHS	0.915	0.763	5.103
NP^3@CHS	0.954	0.841	5.468
NP^4@CHS	0.885	0.726	4.869
Pt/C	0.976	0.840	5.306

Table S3. The comparison of the ORR performance of different reported fullerene-derived carbons in alkaline medium.

Catalyst	E_0 (V)	$E_{1/2}$ (V)	j_L (mA cm^{-2})	Electrolyte	Ref.
NP^3@CHS	0.954	0.841	5.468	0.1M KOH	This work
PD/N-C	0.911	0.833	5.29	0.1M KOH	s11
MFC$_{60}$-130	0.82	0.76	-	0.5M KOH	s12
FMN700	0.93	0.81	-	0.1M KOH	s13
Fe-MFC$_{60}$-150	085	0.78	-	0.5M KOH	s14
Cu(15%)-MFC$_{60}$	0.86	0.76	5.18	0.1M KOH	s15
N,S-PCNFs	0.969	0.837	5.50	0.1M KOH	s16
N,S-PHCNSs-75	0.954	0.827	5.64	0.1M KOH	s17
FPCFs@rGO	0.895	0.762	4.96	0.1M KOH	s18

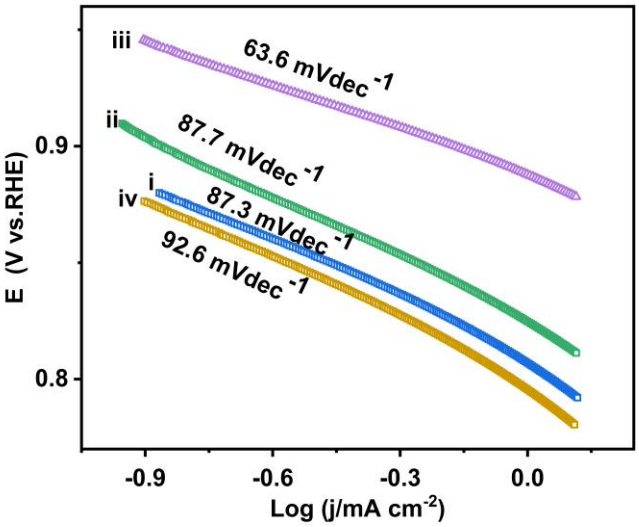

Figure S13. Tafel plots of (i) NP^1@CHS, (ii) NP^2@CHS, (iii) NP^3@CHS and (iv) NP^4@CHS.

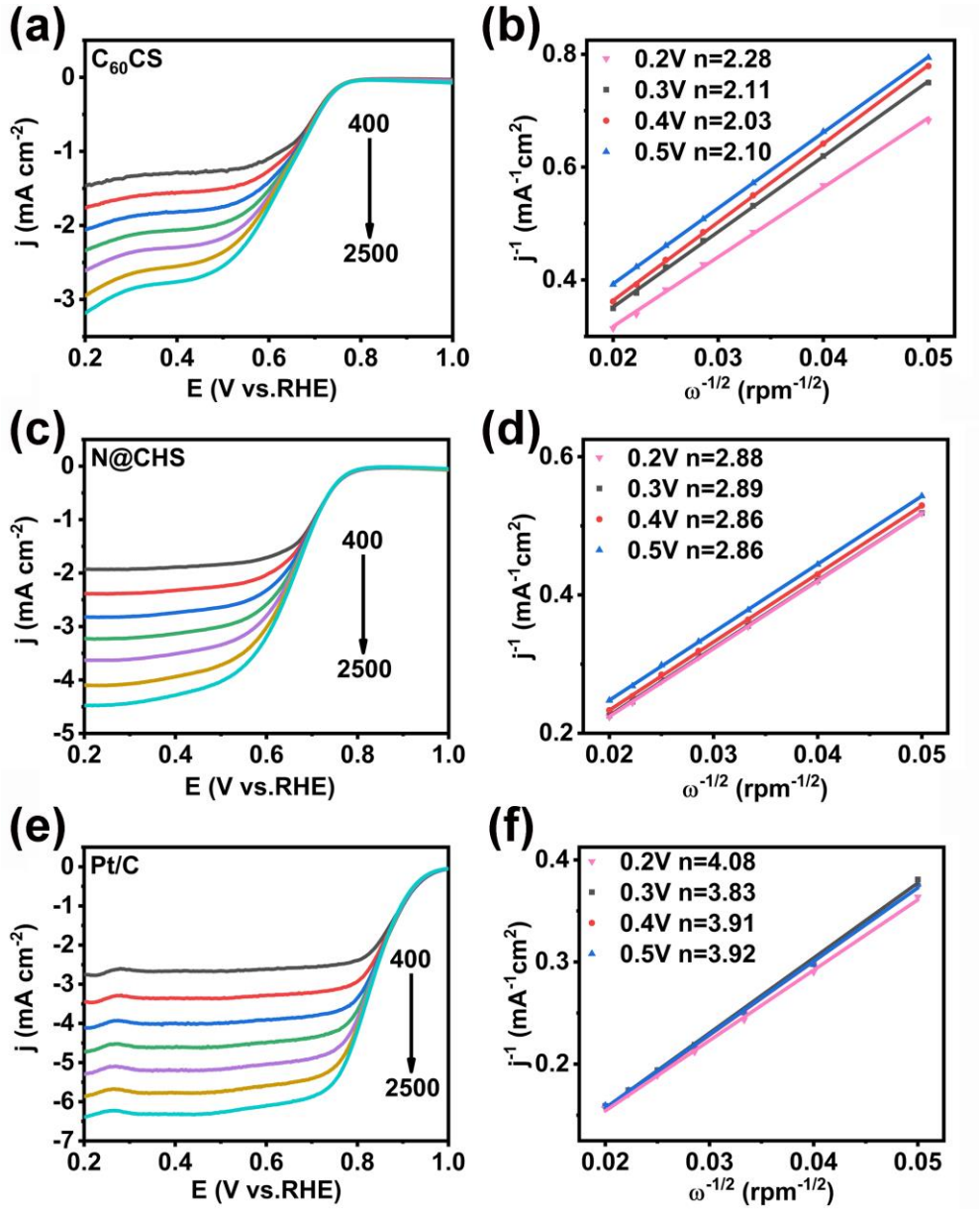

Figure S14. LSV curves of (a) C_{60}CS, (c) N@CHS and (e) Pt/C at different rotation rates (400-2500 rpm). The K-L plots of (b) C_{60}CS, (d) N@CHS and (f) Pt/C.

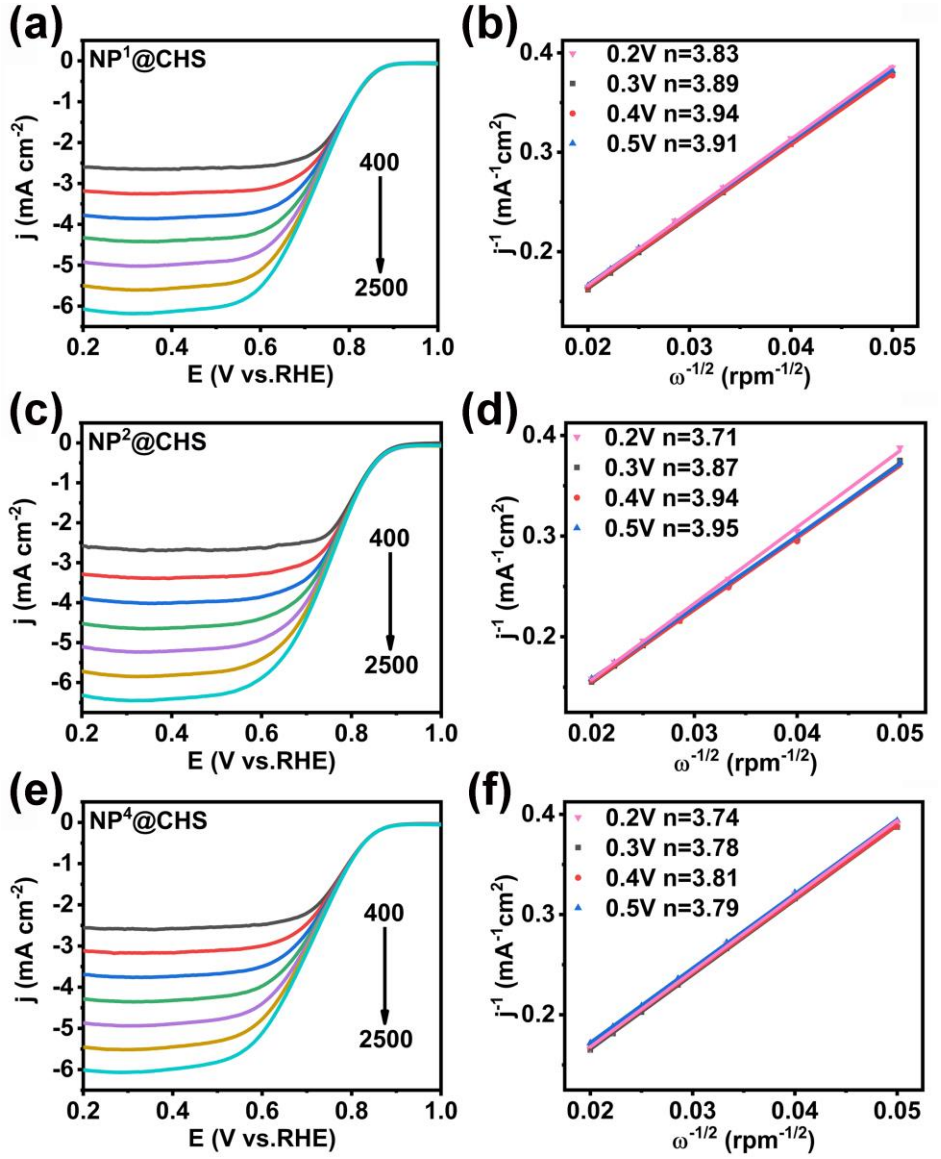

Figure S15. LSV curves of (a) NP^1@CHS, (c) NP^2@CHS and (e) NP^4@CHS at different rotation rates (400-2500 rpm). The K-L plots of (b) NP^1@CHS, (d) NP^2@CHS and (f) NP^4@CHS.

References in supporting information

[s1]. A. D. Becke, Phys. Rev. A, 1988, **38**, 3098.

[s2]. C. Lee, W. Yang, and R. G. Parr, Phys. Rev. B, 1988, **37**, 785.

[s3]. A. D. Becke, *J. Chem. Phys.*, 1993, **98**, 5648.

[s4]. G. A. Petersson, A. Bennett, T. G. Tensfeldt, M. A. Al‐Laham, and W. A. Shirley, *J. Chem. Phys.*, 1988, **89**, 2193.

[s5]. G. A. Petersson and M. A. Al‐Laham, *J. Chem. Phys.*, 1991, **94**, 6081.

[s6]. A. V. Marenich, C. J. Cramer and D. G. Truhlar, *J. Phys. Chem. B*, 2009, **113**, 6378.

[s7]. Y. Zhao and D. G. Truhlar, *Theor. Chem. Account*, 2008, **120**, 215.

[s8]. F. Weigend and R. Ahlrichs, *Phys. Chem. Chem. Phys.*, 2005, **7**, 3297.

[s9]. Gaussian 16, Revision A.03, M. J. Frisch, G. W. Trucks, H. B. Schlegel, G. E. Scuseria, M. A. Robb, J. R. Cheeseman, G. Scalmani, V. Barone, G. A. Petersson, H. Nakatsuji, X. Li, M. Caricato, A. V. Marenich, J. Bloino, B. G. Janesko, R. Gomperts, B. Mennucci, H. P. Hratchian, J. V. Ortiz, A. F. Izmaylov, J. L. Sonnenberg, D. Williams-Young, F. Ding, F. Lipparini, F. Egidi, J. Goings, B. Peng, A. Petrone, T. Henderson, D. Ranasinghe, V. G. Zakrzewski, J. Gao, N. Rega, G. Zheng, W. Liang, M. Hada, M. Ehara, K. Toyota, R. Fukuda, J. Hasegawa, M. Ishida, T. Nakajima, Y. Honda, O. Kitao, H. Nakai, T. Vreven, K. Throssell, J. A. Montgomery, Jr., J. E. Peralta, F. Ogliaro, M. J. Bearpark, J. J. Heyd, E. N. Brothers, K. N. Kudin, V. N. Staroverov, T. A. Keith, R. Kobayashi, J. Normand, K. Raghavachari, A. P. Rendell, J. C. Burant, S. S. Iyengar, J. Tomasi, M. Cossi, J. M. Millam, M. Klene, C. Adamo, R. Cammi, J. W. Ochterski, R. L.

Martin, K. Morokuma, O. Farkas, J. B. Foresman, and D. J. Fox, Gaussian, Inc., Wallingford CT, 2016.

[s10]. A. A. Peterson, F. Abild-Pedersen, F. Studt, J. Rossmeisl and J. K. Nørskov, *Energy Environ. Sci.*, 2010, **3**, 1311.

[s11]. J. Zhu, Y. Huang, W. Mei, C. Zhao, C. Zhang, J. Zhang, I. S. Amiinu and S. Mu, *Angew. Chem., Int. Ed.*, 2019, **58**, 3859-3864.

[s12]. M. R. Benzigar, S. Joseph, H. Ilbeygi, D.-H. Park, S. Sarkar, G. Chandra, S. Umapathy, S. Srinivasan, S. N. Talapaneni, A. Vinu, *Angew. Chem. Int. Ed.* 2018, **57**, 569.

[s13]. Z. Peng, Q. Jiang, P. Peng and F.-F. Li, *Eng. Sci.*, 2021, **14**, 27-38.

[s14]. M. R. Benzigar, S. Joseph, G. Saianand, A.-I. Gopalan, S. Sarkar, S. Srinivasan, D.-H. Park, S. Kim, S. N. Talapaneni, K. Ramadass and A. Vinu, *Microporous Mesoporous Mater.*, 2019, **285**, 21-31.

[s15]. G. Saianand, A. I. Gopalan, J. C. Lee, C. I. Sathish, K. Gopalakrishnan, G. E. Unni, D. Shanbhag, V. Dasireddy, J. Yi, S. Xi, A. H. Al-Muhtaseb and A. Vinu, *Small*, 2020, **16**, e1903937.

[s16]. Z. He, P. Wei, N. Chen, J. Han and X. Lu, *Chem.-Eur. J.*, 2021, **27**, 1423-1429.

[s17]. Z. He, P. Wei, T. Xu, J. Han, X. Gao and X. Lu, *Mater. Chem. Front.*, 2021, **5**, 7873-7882.

[s18]. Z. He, Z. Guo, K. Guo, T. Akasaka and X. Lu, *C-J. Carbon Res.*, 2022, **8**, 13.